



Published in final edited form as:

*Mol Pharm.* 2013 September 3; 10(9): 3296–3303. doi:10.1021/mp300720k.

## Enhanced Cell Death Imaging Using Multivalent Zinc(II)-Bis(dipicolylamine) Fluorescent Probes

Bryan A. Smith<sup>1</sup>, Shuzhang Xiao<sup>1</sup>, Kara M. Harmatys<sup>1</sup>, Erin L. Cole<sup>1</sup>, Adam J. Plaunt<sup>1</sup>, William Wolter<sup>2</sup>, Mark A. Suckow<sup>2</sup>, and Bradley D. Smith<sup>1,\*</sup>

<sup>1</sup>Department of Chemistry and Biochemistry, 236 Nieuwland Science Hall, University of Notre Dame, Notre Dame, IN 46556

<sup>2</sup>Freimann Life Science Center, 400 Galvin Life Science, University of Notre Dame, Notre Dame, IN 46556

### Abstract

There is a clinical need for imaging technologies that can accurately detect cell death in a multitude of pathological conditions. Zinc(II)-bis(dipicolylamine) (Zn<sub>2</sub>BDPA) coordination complexes are known to associate with the anionic phosphatidylserine that is exposed on the surface of dead and dying cells, and fluorescent monovalent Zn<sub>2</sub>BDPA probes are successful cell death imaging agents. This present study compared the membrane targeting ability of two structurally related deep-red fluorescent probes, Bis-Zn<sub>2</sub>BDPA-SR and Tetra-Zn<sub>2</sub>BDPA-SR, with two and four appended Zn<sub>2</sub>BDPA units, respectively. Vesicle and cell microscopy studies indicated that a higher number of Zn<sub>2</sub>BDPA targeting units improved probe selectivity for phosphatidylserine-rich vesicles, and increased probe localization at the plasma membrane of dead and dying cells. The fluorescent probes were also tested in three separate animal models, 1) necrotic prostate tumor rat model, 2) thymus atrophy mouse model, and 3) traumatic brain injury mouse model. In each case there was more Tetra-Zn<sub>2</sub>BDPA-SR accumulation at the site of cell death than Bis-Zn<sub>2</sub>BDPA-SR. The results indicate that multivalent Zn<sub>2</sub>BDPA probes are promising molecules for effective imaging of cell death processes in cell culture and in living subjects.

### Keywords

cell death imaging; multivalency; zinc(II)-bis(dipicolylamine); in vivo fluorescence imaging; phosphatidylserine; squaraine rotaxane

### Introduction

Cell death is a critical process for maintaining normal development and preventing the onset of pathological conditions.<sup>1,2</sup> Disruption of homeostasis, either by excessive or deficient cell death, has been linked to cancer, neurodegenerative disorders, cardiovascular diseases, and auto-immune diseases.<sup>3–5</sup> There is an ongoing research effort to develop imaging and diagnostic agents that can target and identify dead and dying cells, with the goal of

\*smith.115@nd.edu.

#### Conflict of Interest

The authors declare no conflicts of interest.

#### Supporting Information

Titration spectra, additional cell and animal images and image analysis. This material is available free of charge via the Internet at <http://pubs.acs.org>.

producing detection technologies that can evaluate the status of disease or the efficacy of therapeutic intervention. In the case of *in vivo* imaging, various strategies have been developed to target either intracellular or extracellular biomarkers of cell death.<sup>6</sup> One approach is to utilize protein or small molecule imaging probes that have selective affinity for the anionic phospholipid, phosphatidylserine (PS), which is exposed on the plasma membrane surface during cell death processes.<sup>7</sup> We have contributed by developing synthetic molecular probes that are equipped with zinc(II)-bis(dipicolylamine) (Zn<sub>2</sub>BDPA) coordination complexes as PS targeting units.<sup>8–12</sup> The membrane association is mediated by coordination of the probe's zinc cations with the oxyanion groups in the PS head group. Successful *in vivo* optical imaging of cell death using fluorescent Zn<sub>2</sub>BDPA probes has been demonstrated in a variety of animal models, although probe doses have been fairly high because the probes only have moderate affinity for membrane surfaces with exposed PS (low micromolar dissociation constants).<sup>13</sup>

In principle, one way to enhance membrane targeting is to employ multivalency, which has been defined as the interaction of multiple recognition elements on a single scaffold with multiple receptors on a separate system.<sup>14</sup> Multivalent interactions are found extensively in membrane biology and are especially important for recognition and attachment of pathogens to host cells.<sup>15,16</sup> The protein Annexin V exhibits highly selective targeting of anionic cell membranes; due in part to a strong multivalent effect produced by the four repeat units in its molecular structure.<sup>17</sup> With this structural precedence in mind, we decided to prepare fluorescent molecular probes that are appended with multiple copies of Zn<sub>2</sub>BDPA targeting units and determine if they act as improved cell death imaging agents. Recently, we invented squaraine rotaxanes (SR) as a novel class of highly stable and extremely bright fluorescent dyes with deep-red emission wavelengths (650 nm–750 nm) and high suitability for whole-body fluorescence imaging.<sup>18,19</sup> The favorable optical properties are due to the interlocked molecular architecture that surrounds the squaraine fluorophore with a protective macrocycle. We have also developed synthetic methods for attaching multiple targeting groups to a central squaraine rotaxane scaffold and creating multivalent fluorescence imaging probes.<sup>20</sup> Here, we compare the targeting and imaging performance of three squaraine rotaxane probes, the tetravalent Tetra-Zn<sub>2</sub>BDPA-SR, the divalent Bis-Zn<sub>2</sub>BDPA-SR, and non-targeted Tracer-653 (Figure 1). The probes have nearly identical deep-red emission wavelengths that facilitate studies using spectroscopic assays, cell microscopy, and small animal models. Evaluating the same probe molecules in these different experimental settings is an important technical advantage that simplifies data comparison. We have determined probe selectivity for vesicle membranes containing PS, and also evaluated ability to target and image cell death in cell culture and in living animal models. We find that increasing the number of Zn<sub>2</sub>BDPA targeting groups improves probe selectivity for PS-rich vesicle membranes, increases probe localization at the plasma membrane of dead and dying cells, and enhances *in vivo* optical imaging performance in three rodent models of cell death.

## Materials and Methods

### Materials

Culture media and bovine serum albumin (BSA) were purchased from Sigma Aldrich. MDA-MB-231 (ATCC: HB-26) and A549 (ATCC: CCL-185) cells were certified and obtained from the ATCC. POPC (1-palmitoyl-2-oleoyl-*sn*-glycero-3-phosphocholine) and POPS (1-palmitoyl-2-oleoyl-*sn*-glycero-3-phosphoserine) were purchased from Avanti Polar Lipids and stored in CHCl<sub>3</sub> at –20 °C. DiI C<sub>18</sub> (1,1'-dioctadecyl-3,3,3',3'-tetramethylindocarbocyanine perchlorate) was purchased from Invitrogen Inc. The syntheses of Tetra-Zn<sub>2</sub>BDPA-SR, Bis-Zn<sub>2</sub>BDPA-SR, Tracer-653, and Zn<sub>2</sub>BDPA have been reported

previously.<sup>21–24</sup> The three squaraine rotaxane probes absorb at ~653 nm and emit at ~672 nm with essentially the same quantum yield and high chemical stability.

### Vesicle Preparation

An appropriate mixture of phospholipid was dried as a film under vacuum for 1 h. A stock solution of vesicles (10 mM phospholipid) was made by rehydration with HEPES buffer (10 mM HEPES, 137 mM NaCl, 3.2 mM KCl, pH 7.4) at room temperature. Multilamellar vesicles were converted to unilamellar vesicles by extruding 21 times through a polycarbonate Nucleopore filter with 200 nm diameter pores using a Basic LiposoFast device (Avestin).

### FRET Titrations

Small aliquots of fluorescent probe stock solution (0.25 mM in HEPES buffer) were added incrementally to a dispersion of vesicles (10  $\mu$ M total phospholipid, HEPES buffer, pH 7.4) under constant stirring at 25 °C. After each addition, a fluorescence spectrum was acquired from 500–750 nm with excitation at 480 nm. The changes in DiI<sub>C18</sub> fluorescence intensity at 567 nm were plotted and the curves for Bis-Zn<sub>2</sub>BDPA-SR binding were fitted using the “one site total” non-linear regression algorithm within the program *Graphpad Prism 5*. The curves for Tetra-Zn<sub>2</sub>BDPA-SR binding did not fit to any standard association model.

### Cell Microscopy

Brightfield and fluorescence microscopy was performed on a Nikon TE-2000U epifluorescence microscope equipped with a Cy5 filter (ex: 620/60, em: 700/75). Fluorescence images were captured using Metamorph software (Universal) and analyzed using *ImageJ*.

MDA-MB-231 cells were seeded onto a chambered coverslip system. Once the cells reached 80 % confluency, etoposide (15  $\mu$ M) was added to the cells and allowed to incubate at 37 °C for 11 h. The media was removed and HEPES buffer was added to the wells, followed by different probe concentrations. The cells were incubated at 37 °C for 30 min, washed three times with HEPES buffer, then imaged by fluorescence microscopy. A549 lung carcinoma cells were subjected to the same protocol except they were stained with only Tetra-Zn<sub>2</sub>BDPA-SR.

For the vesicle cold block study, MDA-MB-231 cells were seeded onto a chambered coverslip system, and once 80 % confluency was reached they were treated with etoposide (15  $\mu$ M) at 37 °C for 11 h. The media was removed and replaced with HEPES buffer. Tetra-Zn<sub>2</sub>BDPA-SR (1  $\mu$ M) was added to the cells along with 100 fold excess of either POPC:POPS (50:50) or POPC liposomes. The cells were incubated at 37 °C for 30 min, washed three times with HEPES buffer, then imaged by fluorescence microscopy.

### Animal Imaging

All animal handling and imaging procedures were approved by the University of Notre Dame Institutional Animal Care and Use Committee. Epifluorescence animal images were acquired using a Carestream Health In-Vivo Multispectral Imaging System FX equipped with 630  $\pm$  10 nm excitation and 700  $\pm$  20 nm emission filter set.

### Prostate Tumor Rat Models

**Subcutaneous prostate tumor rat model**—Eight-week old Lobund Wistar rats (Freimann Life Science Center; 250 g, n = 4) were injected subcutaneously into the right flank with  $1 \times 10^6$  Prostate Adenocarcinoma III (PAIII) cells suspended in 300  $\mu$ L of DMEM medium. Tumors grew for 14 days prior to probe dosing and imaging. The rats were

anesthetized (1.5 % isoflurane inhalation) and injected intravenously via the tail vein with 20 nmol of either Tetra-Zn<sub>2</sub>BDPA-SR, Bis-Zn<sub>2</sub>BDPA-SR, or Tracer-653 in water. Twenty-four hours after probe injection, the rats were anesthetized and sacrificed. The skin covering the flank of each rat was removed before whole-body fluorescence imaging.

**Spontaneous prostate tumor rat model**—A cohort of 3–4 month old Lobund-Wistar rats (n = 3) were injected intravenously with N-methyl-N-nitrosourea (MNU, 30 mg/kg) followed by subcutaneous implantation of testosterone propionate (25 mg) pellets at 7 d, 60 d, and 120 d post-MNU injection. Once prostate tumors were palpable (typically by 10–12 months of age), the rats were injected intravenously via the tail vein with Tetra-Zn<sub>2</sub>BDPA-SR (20 nmol). Twenty-four hours post-injection, the rats were euthanized by CO<sub>2</sub> asphyxiation and the skin overlying the pelvic-abdominal region was removed to facilitate whole-body fluorescence imaging. Selected tissues were excised and placed on a transparent imaging tray for ex vivo fluorescence imaging.

### Thymus Atrophy Mouse Model

Six cohorts of 8-week old male immunocompetent hairless mice (*SKH-1*, Freimann Life Science Center, ~ 25 g) (n = 4) were given intraperitoneal injections (50 mg/kg) of water soluble dexamethasone (Sigma Aldrich) dissolved in 100  $\mu$ L of distilled water. The time from dexamethasone dosing to sacrifice of the cohort (and its related control cohort) was 42 h with injection of fluorescent probe at 24 h before sacrifice. The fluorescent probe (20 nmol either Tetra-Zn<sub>2</sub>BDPA-SR, Bis-Zn<sub>2</sub>BDPA-SR, or Tracer-653 in water) was injected intravenously via the tail vein. Three additional cohorts of mice (n = 4) were not treated with dexamethasone, but were injected with fluorescent probe (Tetra-Zn<sub>2</sub>BDPA-SR, Bis-Zn<sub>2</sub>BDPA-SR, or Tracer-653). All animals were euthanized by either CO<sub>2</sub> asphyxiation or cervical dislocation under anesthesia. After sacrifice, selected tissues were excised and placed on a transparent imaging tray for ex vivo fluorescence imaging.

### Traumatic Brain Injury Mouse Model

Three cohorts of 4–6 week old immunocompetent hairless mice (male, ~25 g, *SKH-1*) (n = 5) were anesthetized by 2 % isoflurane inhalation. A metal cylinder, with a 3 mm diameter, was pre-cooled in liquid nitrogen and applied to the parietal region of each mouse's head for 60 s. The mice then received a 20 nmol intravenous injection of either Tetra-Zn<sub>2</sub>BDPA-SR, Bis-Zn<sub>2</sub>BDPA-SR, or Tracer-653, and whole-body epi-fluorescence images were acquired immediately after probe injection and at 3, 6, and 24 h time points. For Zn<sub>2</sub>BDPA cold block studies, immunocompetent hairless mice (*SKH-1*, ~25 g, n = 4) were administered a solution of either Zn<sub>2</sub>BDPA in 100  $\mu$ L of 10% DMSO/H<sub>2</sub>O or vehicle control (100  $\mu$ L of 10% DMSO/H<sub>2</sub>O) immediately after cryoinjury. Thirty minutes was allowed to elapse, then the mice were injected retro-orbitally with 20 nmol of either Tetra-Zn<sub>2</sub>BDPA-SR or Bis-Zn<sub>2</sub>BDPA-SR. The concentration of Zn<sub>2</sub>BDPA was 15 fold higher than the effective concentration of Zn<sub>2</sub>BDPA units on the multivalent Tetra-Zn<sub>2</sub>BDPA-SR and Bis-Zn<sub>2</sub>BDPA-SR probes. After twenty-four hours, the mice were anesthetized, sacrificed, and the brains were excised for ex vivo fluorescence imaging.

### Fluorescence Image Analysis

Images were analyzed using *ImageJ* software. The 16-bit images were imported, opened in sequential order, and converted to an image stack. Background subtraction was applied to the images using the rolling ball algorithm. The stack was then converted to a montage and pseudocolored as “Thai” (under the “Lookup Tables” menu). Region of interest (ROI) analysis was performed on each in vivo and ex vivo image by drawing an area around the Target (T) and a same sized area around a suitable Non-Target (NT) location. For the in vivo

tumor imaging studies, the NT site was the contralateral flank, and for the in vivo traumatic brain injury studies, the NT site was on the lower back of the animal. The mean pixel intensities for T and NT regions were measured and plotted using *Graphpad Prism 4*. For ex vivo biodistribution images, ROI analysis of each excised tissue produced a mean pixel intensity. For the Traumatic Brain Injury study,  $I/I_0$  values for the cryoinjury were calculated by measuring the mean pixel intensities at each time point (I) and dividing by the mean pixel intensities at the initial time point ( $I_0$ ).

### Statistical Analysis

Results are depicted as mean  $\pm$  standard error of the mean (SEM). Statistical analysis was performed using a Student's t-test.

### Results

A fluorescence resonance energy transfer (FRET) titration assay was developed to enable direct comparison of probe binding to vesicles with membrane compositions that mimicked the plasma membranes of healthy cells (zwitterionic POPC only) or dead/dying cells (mixture of POPC and anionic POPS). In each case, the vesicles contained 1 mol % of the lipophilic fluorescence energy donor dye DiIC<sub>18</sub> that is excited at 480 nm and emits at 570 nm.<sup>25</sup> Association of squaraine rotaxane probe (acting as FRET acceptor) to the vesicle surface leads to quenching of the DiIC<sub>18</sub> emission (Figure S1). The titration plots in Figure 2a show that Bis-Zn<sub>2</sub>BDPA-SR has moderate affinity for POPC vesicles ( $K_d = 0.43 \pm 0.04$   $\mu$ M) and slightly higher affinity for POPC/POPS vesicles ( $K_d = 0.15 \pm 0.02$   $\mu$ M). In comparison, the Tetra-Zn<sub>2</sub>BDPA-SR with its greater positive charge and increased hydrophilicity exhibited a much higher selectivity for the anionic POPC/POPS vesicles over zwitterionic POPC vesicles (Figure 2b). Quantitative analysis of the Tetra-Zn<sub>2</sub>BDPA-SR titration curves was not possible due to the very weak association with the POPC vesicles and precipitation of the cross-linked POPC/POPS vesicles in the later stages of the titration. But qualitatively, the curves show that the higher selectivity exhibited by Tetra-Zn<sub>2</sub>BDPA-SR (compared to Bis-Zn<sub>2</sub>BDPA-SR) is not due to an increase in POPC/POPS affinity but instead to substantially reduced POPC affinity. As expected, the control probe, Tracer-653, had negligible interaction with the vesicles (Figure 2c).

Cell microscopy studies primarily employed cultures of MDA-MB-231 breast cancer cells, and cell death was induced by preliminary treatment with etoposide, a topoisomerase inhibitor.<sup>26</sup> As expected, the Tracer-653 did not associate with healthy or dead cells. The Tetra-Zn<sub>2</sub>BDPA-SR and Bis-Zn<sub>2</sub>BDPA-SR also did not stain healthy cells, but both probes selectively targeted dead and dying cells (Figure S2). As shown in Figure 3, there was a marked difference in cell distribution; the Tetra-Zn<sub>2</sub>BDPA-SR localized strongly at the plasma membrane whereas the Bis-Zn<sub>2</sub>BDPA-SR distributed throughout the cytosol. Additional multicolor fluorescence imaging studies included the blue-emitting, nucleic acid stain, SYTOX Blue. Since the dye is membrane impermeable, it only stains necrotic cells that have a compromised plasma membrane. As illustrated in Figure 4 and Figure S3, the staining combination observed with a binary mixture of Zn<sub>2</sub>BDPA probe and SYTOX Blue allowed distinction of healthy, apoptotic, and necrotic cells.

The strong localization of Tetra-Zn<sub>2</sub>BDPA-SR at the plasma membrane enabled high contrast imaging of dead and dying cells at significantly lower concentrations than the 10  $\mu$ M that is typically used for monovalent Zn<sub>2</sub>BDPA fluorescent probes. Indeed, effective plasma membrane staining of dead/dying MDA-MB-231 cells and also A549 lung carcinoma cells was observed using Tetra-Zn<sub>2</sub>BDPA-SR at the low concentration of 500 nM (Figure S4). Moreover, the staining with Tetra-Zn<sub>2</sub>BDPA-SR allowed visualization of apoptotic bodies that were external to the cell surface.

Evidence that dead/dying cell staining by Tetra-Zn<sub>2</sub>BDPA-SR was a membrane targeting process was gained by conducting a cold block study that used vesicles to competitively inhibit association of Tetra-Zn<sub>2</sub>BDPA-SR to etoposide-treated MDA-MB-231 cells. As seen in Figure S5a, a 100-fold excess of POPC and POPC:POPS (1:1) vesicles inhibited Tetra-Zn<sub>2</sub>BDPA-SR staining of cell death. Quantification of the fluorescence micrographs (Figure S5b) confirmed that POPC:POPS vesicles were more effective than the POPC vesicles at blocking cell targeting of Tetra-Zn<sub>2</sub>BDPA-SR, in agreement with the probe/vesicle affinity differences noted in Figure 2.

Repeated attempts were made to evaluate the cell staining by flow cytometry. Separate samples of healthy and etoposide-treated MDA-MB-231 cells were incubated with various concentrations of Bis-Zn<sub>2</sub>BDPA-SR or Tetra-Zn<sub>2</sub>BDPA-SR and then the cells were released into solution by treatment with trypsin. Histograms of the cells treated with Bis-Zn<sub>2</sub>BDPA-SR consistently showed selective staining of a population of dead/dying cells induced by the etoposide. However, consistent flow cytometry data could not be gained when the cells were treated with Tetra-Zn<sub>2</sub>BDPA-SR. The major technical problem was cross-linking of the dead/dying cells after treatment with trypsin, an observation that is consistent with the probe-induced precipitation of POPC/POPS vesicles described above, and also with the cell fluorescence images in Figure 3 showing extensive localization of the Tetra-Zn<sub>2</sub>BDPA-SR at the surface of the dead/dying cells. We conclude that the multivalent Tetra-Zn<sub>2</sub>BDPA-SR is a highly effective fluorescent probe for staining dead/dying cells that are adhered to surfaces but it is problematic for analyses of cells or vesicles that are dispersed in solution due to cross-linking effects.

The *in vivo* targeting abilities of the probes were evaluated in three different animal models of cell death that we have previously shown can be imaged using fluorescent Zn<sub>2</sub>BDPA probes. The first study used two versions of a prostate tumor rat model that is known to develop necrotic foci.<sup>9</sup> A subcutaneous tumor model was created by injecting PAIII prostate cancer cells subcutaneously into the flanks of Lobund-Wistar rats and allowing them to grow for 14 days to ensure that areas of cell death had developed within the tumor. Rats were then injected with 20 nmol of either Tetra-Zn<sub>2</sub>BDPA-SR, Bis-Zn<sub>2</sub>BDPA-SR, or Tracer-653. After 24 h the rats were sacrificed and the skin covering the flanks of the rats was removed to allow semi-quantitative imaging of probe accumulation within the tumors. As seen in Figure 5a, tumors were easily visualized as target sites (T) in animals injected with Tetra-Zn<sub>2</sub>BDPA-SR and Bis-Zn<sub>2</sub>BDPA-SR, while Tracer-653 showed minor tumor accumulation. Region of interest (ROI) analysis showed that the Tetra-Zn<sub>2</sub>BDPA-SR had the highest T/NT value ( $8.57 \pm 1.67$ ) compared to Bis-Zn<sub>2</sub>BDPA-SR ( $4.22 \pm 0.28$ ) and Tracer-653 ( $2.56 \pm 0.21$ ) (Figure 5b). An additional set of imaging studies using a more clinically relevant spontaneous prostate tumor rat model showed similar high tumor accumulation of Tetra-Zn<sub>2</sub>BDPA-SR (Figure S6).

The second animal model study used immunocompetent mice with intraperitoneal injections of dexamethasone to induce extensive thymocyte cell death and thymus atrophy.<sup>11,27-29</sup> The model is technically straightforward to conduct, with excellent reproducibility and high animal throughput, making it an ideal animal model for validating cell death imaging probes. Tetra-Zn<sub>2</sub>BDPA-SR, Bis-Zn<sub>2</sub>BDPA-SR, and Tracer-653 were injected intravenously into mice at 18 h after treatment with dexamethasone or vehicle control and the mice were sacrificed at 24 h after probe injection. Images of the excised thymi and the corresponding mean pixel intensities determined by ROI analysis are shown in Figure 6. The average mean pixel intensity for Tetra-Zn<sub>2</sub>BDPA-SR accumulation in the thymi taken from treated animals was 2.5 and 5.5 fold greater than Bis-Zn<sub>2</sub>BDPA-SR and Tracer-653, respectively. Moreover, both Zn<sub>2</sub>BDPA fluorescent probes exhibited higher accumulation than

Tracer-653 in thymi from non-treated control mice, consistent with the probe's better ability to target basal levels of thymocyte cell death.

The third animal study was a model of traumatic brain injury that induced rapid breakdown of the blood-brain barrier and tissue damage via application of a pre-cooled rod to the head of a mouse.<sup>12,30–32</sup> In short, three separate cohorts of immunocompetent mice ( $n = 4$ ) were anesthetized by isoflurane inhalation. A metal cylinder with a 3 mm diameter was pre-cooled in liquid nitrogen and applied to each mouse's head for 60 s. The mice were injected intravenously with either Tetra-Zn<sub>2</sub>BDPA-SR, Bis-Zn<sub>2</sub>BDPA-SR, or Tracer-653 and subjected to in vivo epi-fluorescence imaging at 0 h, 3 h, 6 h, and 24 h after probe dosage. The in vivo images showed early accumulation of Tetra-Zn<sub>2</sub>BDPA-SR and Bis-Zn<sub>2</sub>BDPA-SR at the site of cryoinjury, and rapid clearance of Tracer-653 (Figure S5). Quantitative ROI analysis of the in vivo images showed that Tetra-Zn<sub>2</sub>BDPA-SR and Bis-Zn<sub>2</sub>BDPA-SR exhibited similar T/NT values over the first six hours (Figure S6). But at the 24 h time point there were two apparent differences, (a) more of the Tetra-Zn<sub>2</sub>BDPA-SR remained in the animal brain (Figure 7a and Fig. S7), and (b) T/NT for Tetra-Zn<sub>2</sub>BDPA-SR ( $4.78 \pm 0.33$ ) at the site of cryoinjury was significantly higher than Bis-Zn<sub>2</sub>BDPA-SR ( $2.12 \pm 0.12$ ) (Figure S8). After the 24 h time point, the mice were anesthetized, sacrificed, and the brains were excised for ex vivo imaging. The brains from cryoinjured mice treated with Tracer-653 showed weak and homogenous staining. In contrast, the brains from cryoinjured mice dosed with Tetra-Zn<sub>2</sub>BDPA-SR and Bis-Zn<sub>2</sub>BDPA-SR showed localized staining at the injury site (Figure 7b) with the Tetra-Zn<sub>2</sub>BDPA-SR images producing higher mean pixel intensities suggesting higher probe concentration.

The importance of the Zn<sub>2</sub>BDPA affinity units for in vivo targeting was confirmed by a cold block experiment that inhibited probe accumulation at the site of cryoinjury. The cold block was achieved by administering a 15-fold molar excess dose of non-fluorescent Zn<sub>2</sub>BDPA (structure in Figure 1) immediately after cryoinjury. Thirty minutes was allowed to elapse before intravenous injection of Tetra-Zn<sub>2</sub>BDPA-SR or Bis-Zn<sub>2</sub>BDPA-SR and the mice were sacrificed 24 h later. The Zn<sub>2</sub>BDPA cold block inhibited Tetra-Zn<sub>2</sub>BDPA-SR and Bis-Zn<sub>2</sub>BDPA-SR targeting by approximately 50 % compared to a control dose of the vehicle (Figure S10).

## Discussion

This study compared three fluorescent probes; Bis-Zn<sub>2</sub>BDPA-SR with two Zn<sub>2</sub>BDPA units, Tetra-Zn<sub>2</sub>BDPA-SR with four Zn<sub>2</sub>BDPA units, and Tracer-653 (Figure 1). The fluorescent squaraine rotaxane scaffold that is common to each probe is lipophilic and previous studies have shown that it readily inserts into bilayer membranes.<sup>21</sup> Probe lipophilicity is diminished by attaching polar functional groups to the structural periphery. In the case of Tracer-653 the high surface density of zwitterionic groups leads to negligible affinity for biological surfaces.<sup>22</sup> Membrane association of Bis-Zn<sub>2</sub>BDPA-SR is driven by a combination of electrostatic and hydrophobic effects. There is considerable association with zwitterionic POPC vesicles and only three times higher affinity for anionic POPC/POPS vesicles. In comparison, the membrane targeting of Tetra-Zn<sub>2</sub>BDPA-SR is dominated by electrostatic interactions and although there is no apparent increase in probe affinity for POPC/POPS vesicles there is greatly reduced affinity for POPC vesicles (Figure 2). This finding highlights an insightful point concerning the molecular design of multivalent Zn<sub>2</sub>BDPA probes. Increasing the number of cationic Zn<sub>2</sub>BDPA units may not necessarily increase a probe's affinity for anionic membranes because the structural change may produce a compensating loss in attractive hydrophobic probe/membrane interactions. But an increase in membrane selectivity is a generally expected outcome. In this present case, the structural change from divalent Bis-Zn<sub>2</sub>BDPA-SR to tetravalent Tetra-Zn<sub>2</sub>BDPA-SR greatly

increased probe selectivity for PS-rich anionic vesicle membranes (mimic of dead/dying cells) over zwitterionic membranes (mimic of healthy cells).

The cell microscopy results showed that both cationic probes selectively targeted dead and dying cells over healthy cells, but the cell staining patterns reflected the inherent difference in membrane selectivity. The tetravalent Tetra-Zn<sub>2</sub>BDPA-SR, with its eight zinc cations, localized strongly at the anionic plasma membranes of both apoptotic and necrotic cells, and was an effective fluorescent stain even at submicromolar concentrations (Figure S4). In contrast the divalent Bis-Zn<sub>2</sub>BDPA-SR distributed throughout the cytosol. The intracellular staining of necrotic cells was expected considering the high cell permeability and the modest membrane selectivity of the Bis-Zn<sub>2</sub>BDPA-SR. An ability to penetrate the intact plasma membrane of apoptotic cells is notable but not a unique finding. A select group of small molecules is known to be transported by a channel protein that becomes activated during apoptosis.<sup>33</sup> The same channel transport process is unlikely to be operating here. Rather, the structure of Bis-Zn<sub>2</sub>BDPA-SR has enough cationic charge and lipophilicity to selectively bind the anionic PS that is exposed on the surface of the apoptotic cell plasma membrane and subsequently diffuse through the membrane to the cytosol. We have observed this type of membrane permeation behavior before with related Zn<sub>2</sub>BDPA structures that have a similar mixture of moderate cationic charge and lipophilicity.<sup>34</sup>

The three fluorescent probes were tested in three separate animal models of cell death, namely, necrotic prostate tumor rat model, thymus atrophy mouse model, and traumatic brain injury mouse model. Each animal model exhibits different cell death features with distinct pharmacokinetics and anatomical barriers; thus combined, the animal models provide a broad test of probe imaging performance. The cell death target sites for two of the models (rat prostate tumor and mouse thymus atrophy) were relatively deep inside the animal and non-invasive in vivo fluorescence imaging was not feasible. Thus, we imaged the animals at one time point, *i.e.*, 24 h after sacrifice, with removal of the skin to improve image quantification (Figures 5 and 6). With both animal models, the imaging showed that the amount of probe accumulation at the site of cell death was Tetra-Zn<sub>2</sub>BDPA-SR > Bis-Zn<sub>2</sub>BDPA-SR >> Tracer-653.

The third cell death model was a traumatic brain injury mouse model and the superficial target site allowed longitudinal fluorescence imaging of living animals. Initially, all three probes localized rapidly to the site of brain injury due to passive diffusion through the disrupted blood-brain-barrier. As expected, washout of Tracer-653 was quite fast and complete within 1 h. After 24 h, there was almost complete clearance of Bis-Zn<sub>2</sub>BDPA-SR but a significant amount of Tetra-Zn<sub>2</sub>BDPA-SR remained at the brain injury site (Figure 7). This result suggests that Tetra-Zn<sub>2</sub>BDPA-SR has higher affinity for the dead and dying cells due a slower rate of dissociation from the cell membrane surface. Support for this picture was gained from the ex vivo brain images which were obtained 24 h after probe dosing (Figure 7b). They showed tighter localization of Tetra-Zn<sub>2</sub>BDPA-SR to the cryoinjury site than Bis-Zn<sub>2</sub>BDPA-SR.

Inspection of the in vivo longitudinal images of mice with brain injury indicates that the Tetra-Zn<sub>2</sub>BDPA-SR signal at the cryoinjury site increases significantly over the first three hours (Figure S9). This imaging effect could be due to a temporal increase in cell death, or to physiological changes caused by the local brain trauma such as increased perfusion or edema. However, these factors were ruled out in a previous study that noted the same imaging effect using a monovalent Zn<sub>2</sub>BDPA probe.<sup>11</sup> An alternative explanation considers the role of PS on the cell surface as a biomarker that triggers recognition and subsequent cell clearance by phagocytes.<sup>35</sup> PS-binding molecules such as Annexin V are known to inhibit clearance of dead and dying cells by masking PS.<sup>36</sup> Thus, it is possible that Zn<sub>2</sub>BDPA



probes can block dead cell clearance by the innate immune system, causing build up of fluorescent Zn<sub>2</sub>BDPA-labeled cells at the injury site. Additional studies are needed to test this immune modulation hypothesis. If correct, it raises the idea of masking PS with multivalent Zn<sub>2</sub>BDPA probes as a strategy to produce novel anticancer treatments.<sup>37</sup>

## Conclusions

Zn<sub>2</sub>BDPA coordination complexes are known to associate with the PS that is exposed on the surface of dead and dying cells, and fluorescent monovalent Zn<sub>2</sub>BDPA probes act as cell death imaging agents. The results of this study support the general hypothesis that increasing the number of Zn<sub>2</sub>BDPA units appended to a fluorescent probe improves the probe's cell death targeting ability. Vesicle titration assays showed that Tetra-Zn<sub>2</sub>BDPA-SR exhibited higher selectivity than Bis-Zn<sub>2</sub>BDPA-SR for anionic POPC/POPS vesicles (mimic of dead/dying cell membranes) over zwitterionic POPC vesicles (mimic of healthy cell membranes). Cell microscopy studies demonstrated that both probes selectively targeted dead and dying cells, but there was a marked difference in cell distribution. The Tetra-Zn<sub>2</sub>BDPA-SR localized strongly at the cell plasma membrane whereas the Bis-Zn<sub>2</sub>BDPA-SR distributed throughout the cytosol. The fluorescent probes were tested in three separate animal models, and in each case there was more Tetra-Zn<sub>2</sub>BDPA-SR accumulation at the site of cell death than Bis-Zn<sub>2</sub>BDPA-SR. Taken together, the results show that deep-red fluorescent multivalent Zn<sub>2</sub>BDPA-SR probes are effective optical imaging agents for visualizing cell death processes in cultured samples and living subjects.

## Supplementary Material

Refer to Web version on PubMed Central for supplementary material.

## Acknowledgments

We are grateful for funding support from NIH grants R01GM059078 (B.D.S.) and T32GM075762 (B.A.S.), and the Notre Dame Integrated Imaging Facility. We thank Sarah Chapman in the NDIIF for technical assistance.

## References

1. Vaux DL, Korsmeyer SJ. Cell death in development. *Cell*. 1999; 96:245–254. [PubMed: 9988219]
2. Thompson CB. Apoptosis in the pathogenesis and treatment of disease. *Science*. 1995; 267:1456–1462. [PubMed: 7878464]
3. Reed JC. Dysregulation of apoptosis in cancer. *J Clin Oncol*. 1999; 17:2941–2953. [PubMed: 10561374]
4. Mattson MP. Apoptosis in neurodegenerative disorders. *Nat Rev Mol Cell Bio*. 2000; 1:120–129. [PubMed: 11253364]
5. Konstantinidis K, Whelan RS, Kitsis RN. Mechanisms of cell death in heart disease. *Arterioscler Thromb Vas Biol*. 2012; 32:1552–1562.
6. Blankenberg FG, Strauss HW. Recent advances in the molecular imaging of programmed cell death: part I-pathophysiology and radiotracers. *J Nucl Med*. 2012;10.2967/jnumed.112.108944
7. Smith BA, Smith BD. Biomarkers and molecular probes for cell death imaging and targeted therapeutics. *Bioconjugate Chem*. 2012; 23:1989–2006.
8. Hanshaw RG, Lakshmi C, Lambert TN, Johnson JR, Smith BD. Fluorescent detection of apoptotic cells by using zinc coordination complexes with a selective affinity for membrane surfaces enriched with phosphatidylserine. *ChemBioChem*. 2005; 6:2214–2220. [PubMed: 16276499]
9. Smith BA, Akers WJ, Leevy WM, Lampkins AJ, Xiao S, Wolter W, Suckow MA, Achilefu S, Smith BD. Optical imaging of mammary and prostate tumors in living animals using a synthetic near infrared zinc (II)-dipiclylamine probe for anionic cell surfaces. *J Am Chem Soc*. 2010; 132:67–69. [PubMed: 20014845]

10. Smith BA, Gammon ST, Xiao S, Wang W, Chapman S, McDermott R, Suckow MA, Johnson JR, Piwnica-Worms D, Gokel GW, Smith BD, Leevy WM. In vivo optical imaging of acute cell death using a near-infrared fluorescent zinc-dipicolylamine probe. *Mol Pharm.* 2011; 8:583–590. [PubMed: 21323375]
11. Smith BA, Xiao S, Wolter W, Wheeler J, Suckow MA, Smith BD. In vivo targeting of cell death using a synthetic fluorescent molecular probe. *Apoptosis.* 2011; 16:722–731. [PubMed: 21499791]
12. Smith BA, Xie BW, van Beek ER, Que I, Blankevoort V, Xiao S, Cole EL, Hoehn M, Kaijzel EL, Löwik CW, Smith BD. Multicolor fluorescence imaging of traumatic brain injury in a cryolesion mouse model. *ACS Chem Neurosci.* 2012; 3:530–537. [PubMed: 22860222]
13. Lakshmi C, Hanshaw RG, Smith BD. Fluorophore linked zinc (II)dipicolylamine coordination complexes as sensors for phosphatidylserine containing membranes. *Tetrahedron.* 2004; 60:11307–11315.
14. Englund EA, Wang D, Fujigaki H, Sakai H, Micklitsch CM, Ghirlando R, Martin-Manso G, Pendrak ML, Roberts DD, Durell SR, Appella DH. Programmable multivalent display of receptor ligands using peptide nucleic acid nanoscaffolds. *Nat Commun.* 2012; 3:614. [PubMed: 22233624]
15. Collins BE, Paulson JC. Cell surface biology mediated by low affinity multivalent protein-glycan interactions. *Curr Opin Chem Biol.* 2004; 8:617–625. [PubMed: 15556405]
16. Krachler AM, Ham H, Orth KP. Outer membrane adhesion factor multivalent adhesion molecule 7 initiates host cell binding during infection by gram-negative pathogens. *Proc Natl Acad Sci US A.* 2011; 108:11614–11619.
17. Lambert TN, Smith BD. Synthetic receptors for phospholipid headgroups. *Coord Chem Rev.* 2003; 240:129–141.
18. Gassensmith JJ, Baumes JM, Smith BD. Discovery and early development of squaraine rotaxanes. *Chem Commun.* 2009; 42:6329–6338.
19. White AG, Fu N, Leevy WM, Lee JJ, Blasco MA, Smith BD. Optical imaging of bacterial infection in living mice using deep-red fluorescent squaraine rotaxane probes. *Bioconjugate Chem.* 2010; 21:1297–1304.
20. Xiao S, Fu N, Peckham K, Smith BD. Efficient synthesis of fluorescent squaraine rotaxane dendrimers. *Org Lett.* 2010; 12:140–143. [PubMed: 19957971]
21. Johnson JR, Fu N, Arunkumar E, Leevy WM, Gammon ST, Piwnica-Worms D, Smith BD. Squaraine rotaxanes: superior substitutes for Cy-5 in molecular probes for near-infrared fluorescence cell imaging. *Angew Chem Int Ed.* 2007; 46:5528–5531.
22. Cole EL, Arunkumar E, Xiao S, Smith BA, Smith BD. Water-soluble, deep-red fluorescent squaraine rotaxanes. *Org Biomol Chem.* 2012; 10:5769–5773. [PubMed: 22159917]
23. Kawahara SI, Uchimaru T. Dinucleotide hydrolysis promoted by dinuclear Zn complexes – the effect of the distance between Zn ions in the complexes on the hydrolysis rate. *Eur J Inorg Chem.* 2001; 9:2437–2442.
24. Xiao S, Turkyilmaz S, Smith BD. Convenient synthesis of multivalent zinc (II)-dipicolylamine complexes for molecular recognition. *Tetrahedron Lett.* 2013; 54:861–864. [PubMed: 23459472]
25. White AG, Gray BD, Pak KY, Smith BD. Deep-red fluorescent imaging probe for bacteria. *Bioorg Med Chem Lett.* 2012; 22:2833–2836. [PubMed: 22424976]
26. Bockbrader KM, Tan M, Sun Y. A small molecule Smac-mimic compound induces apoptosis and sensitizes TRAIL- and etoposide-induced apoptosis in breast cancer cells. *Oncogene.* 2005; 24:7381–7388. [PubMed: 16044155]
27. Sun XM, Dinsdale D, Snowden RT, Cohen GM, Skilleter DN. Characterization of apoptosis in thymocytes isolated from dexamethasone-treated rats. *Biochem Pharmacol.* 1992; 44:2131–2137. [PubMed: 1472078]
28. Ahmed SA, Sriranganathan N. Differential effects of dexamethasone on the thymus and spleen: alterations in programmed cell death, lymphocyte subsets and activation of T cells. *Immunopharmacology.* 1994; 28:55–66. [PubMed: 7523333]
29. Ichiyoshi H, Kiyozuka Y, Kishimoto Y, Fukuhara S, Tsubura A. Massive telomere loss and telomerase RNA expression in dexamethasone-induced apoptosis in mouse thymocytes. *Exp Mol Pathol.* 2003; 75:178–186. [PubMed: 14516782]

30. Murakami K, Kondo T, Yang G, Chen SF, Morita-Fujimura Y, Chan PH. Cold injury in mice: a model to study mechanisms of brain edema and neuronal apoptosis. *Prog Neurobiol.* 1999; 57:289–299. [PubMed: 10096842]
31. Raslan F, Schwarz T, Meuth SG, Austinat M, Bader M, Renne T, Roosen K, Stoll G, Siren AL, Kleinschnitz C. Inhibition of bradykinin receptor B1 protects mice from focal brain injury by reducing blood-brain barrier leakage and inflammation. *J Cereb Blood Flow Metab.* 2010; 30:1477–1486. [PubMed: 20197781]
32. Stoffel M, Blau C, Reinl H, Breidt J, Gersonde K, Baethmann A, Plesnila N. Identification of brain tissue necrosis by MRI: validation by histomorphometry. *J Neurotrauma.* 2004; 21:733–740. [PubMed: 15253801]
33. Chekeni FB, Elliot MR, Sandilos JK, Walk SF, Kinchen JM, Lazarowski ER, Armstrong AJ, Penuela S, Laird DW, Salvesen GS, Isakson BE, Bayliss DA, Ravichandran KS. Pannexin 1 channels mediate “find-me” signal release and membrane permeability during apoptosis. *Nature.* 2010; 467:863–867. [PubMed: 20944749]
34. Jiang H, O’Neil EJ, DiVittorio KM, Smith BD. Anion mediated phase transfer of zinc (II) coordinated tyrosine derivatives. *Org Lett.* 2005; 7:3013–3017. [PubMed: 15987193]
35. Ravichandran KS. Beginnings of a good apoptotic meal: the find-me and eat-me signaling pathways. *Immunity.* 2011; 35:445–455. [PubMed: 22035837]
36. Munoz LE, Franz S, Pausch F, Furnrohr B, Sheriff A, Vogt B, Kern PM, Baum W, Stach C, von Laer D, Brachvogel B, Poschl E, Herrmann M, Gaipf US. The influence on the immunomodulatory effects of dying and dead cells of Annexin V. *J Leukocyte Biol.* 2007; 81:6–14. [PubMed: 17005907]
37. Frey B, Schildkopf P, Rödel F, Weiss EM, Munoz LE, Herrmann M, Fietkau R, Gaipf US. Annexin A5 renders dead tumor cells immunogenic—implications for multimodal cancer therapies. *J Immunotoxicol.* 2009; 6:209–216. [PubMed: 19908939]

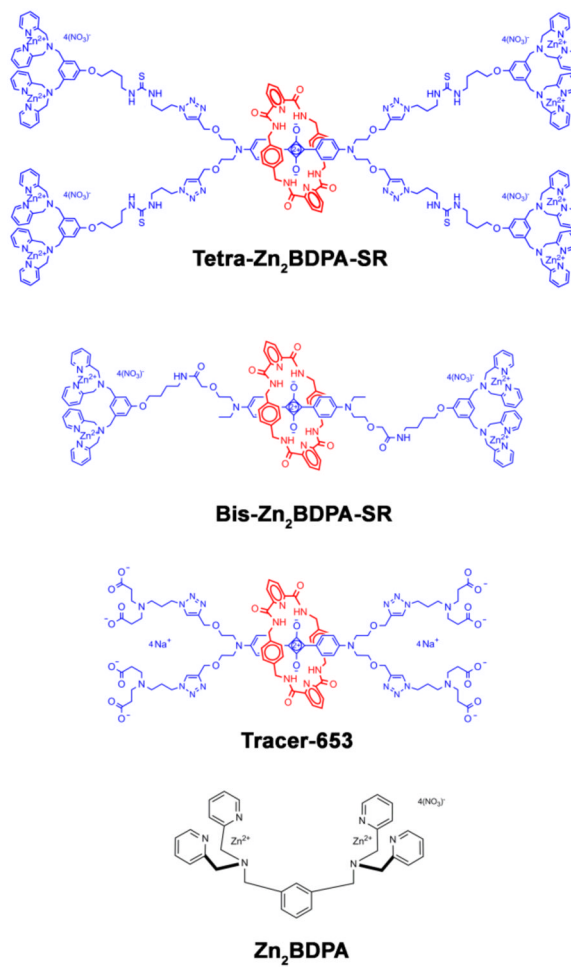


**Figure 1.**  
Chemical structures.

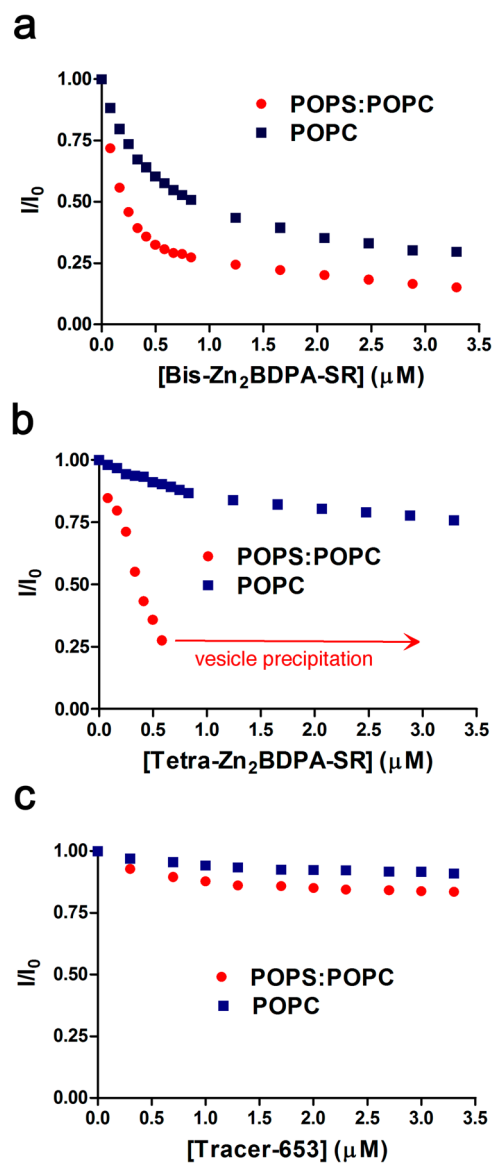


**Figure 2.** Titration of squaraine rotaxane probe as energy acceptor to vesicles (10  $\mu$ M total phospholipid, HEPES buffer, pH 7.4) containing 1 mol % of the energy donor DiIC<sub>18</sub> and either 99 % POPC, or 49:50 % POPS:POPC mixture. Graphs show change in DiIC<sub>18</sub> fluorescence intensity (ex: 480 nm, em: 567 nm) due to FRET quenching by: (a) Bis-Zn<sub>2</sub>BDPA-SR, (b) Tetra-Zn<sub>2</sub>BDPA-SR, (c) Tracer-653.

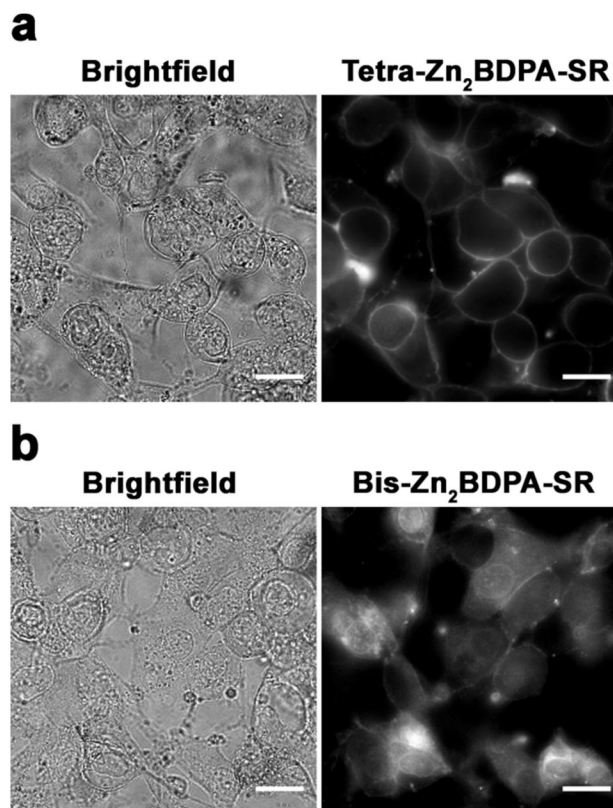


**Figure 3.** Brightfield and deep-red fluorescence micrographs of dead/dying MDA-MB-231 cells stained with either Tetra-Zn<sub>2</sub>BDPA-SR (**a**) or Bis-Zn<sub>2</sub>BDPA-SR (**b**). The cells were initially treated with etoposide (15  $\mu$ M) for 11 hr, incubated with 10  $\mu$ M of probe for 30 min at 37  $^{\circ}$ C, then washed with HEPES buffer. Scale bar = 30  $\mu$ m.

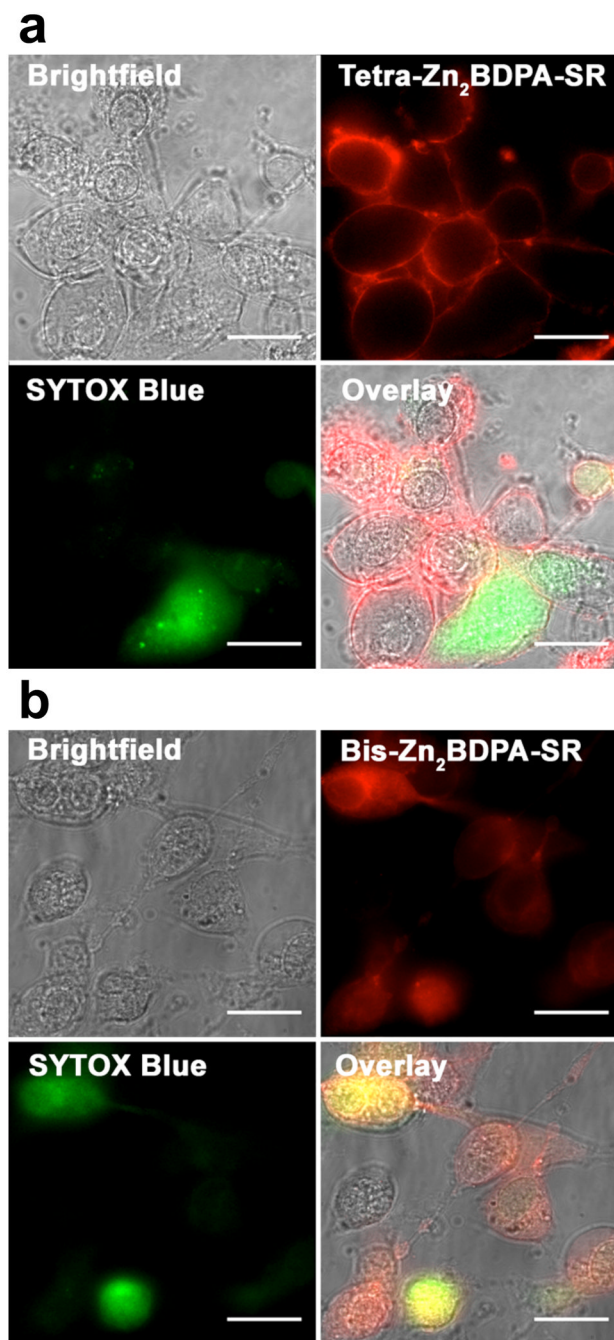


**Figure 4.** Representative brightfield and fluorescence micrographs showing dead/dying MDA-MB-231 cells after treatment with a binary mixture of nucleic acid stain SYTOX Blue (5  $\mu$ M) and either Tetra-Zn<sub>2</sub>BDPA-SR (**a**) or Bis-Zn<sub>2</sub>BDPA-SR (**b**) (10  $\mu$ M). In each case, the cells were initially treated with etoposide (15  $\mu$ M) for 11 hr, incubated with the probes for 30 min at 37 °C, then washed with HEPES buffer. Scale bar = 30  $\mu$ m. Healthy cells are unstained, cells only stained red are apoptotic, and cells stained both red and green are necrotic.

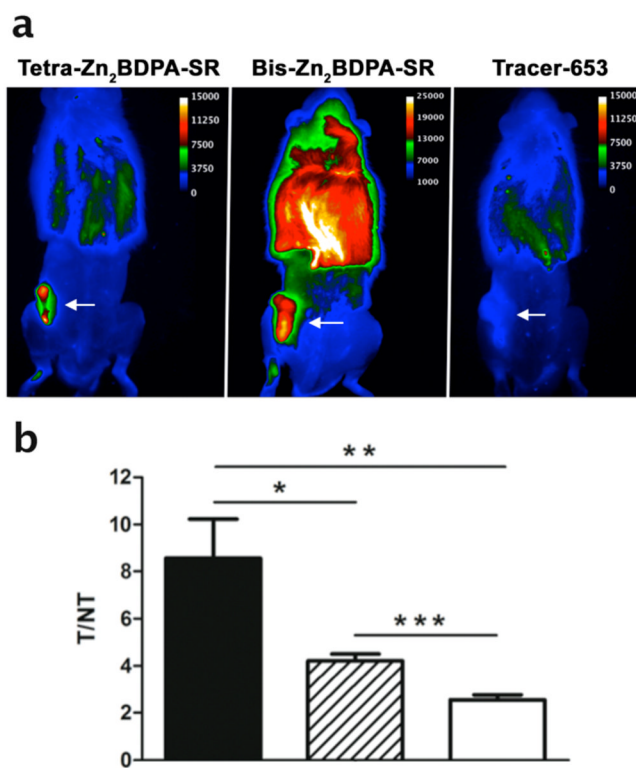


**Figure 5.** Representative fluorescence images of Tetra-Zn<sub>2</sub>BDPA-SR, Bis-Zn<sub>2</sub>BDPA-SR, and Tracer-653 accumulation in a subcutaneous prostate tumor rat model with tumor indicated by arrow (**a**). Comparison of Tetra-Zn<sub>2</sub>BDPA-SR (black bar), Bis-Zn<sub>2</sub>BDPA-SR (dashed bar), and Tracer-653 (white bar) targeting to prostate tumors (**b**). Target to non-target (T/NT) values were calculated by region of interest analysis of whole-body images. \*  $P < 0.05$ , \*\*  $P < 0.02$ , \*\*\*  $P < 0.003$ .  $N = 4$ .



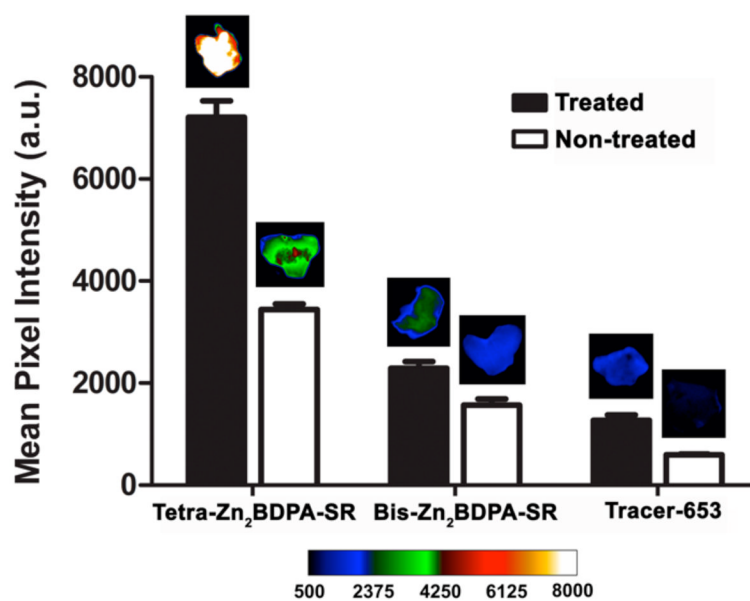


**Figure 6.** Mean pixel intensities of excised thymi from mice that were treated with dexamethasone (50 mg/kg) and dosed with either Tetra-Zn<sub>2</sub>BDPA-SR, Bis-Zn<sub>2</sub>BDPA-SR, or Tracer-653 (20 nmol). Ex vivo images were acquired 24 h after probe administration. N = 4.

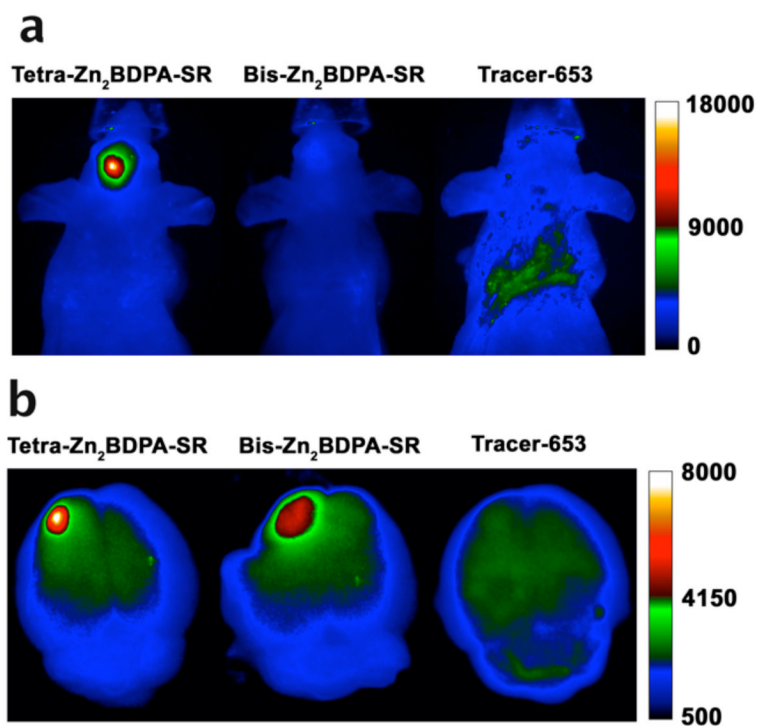


**Figure 7.** Images of traumatic brain injury in a mouse model. Representative in vivo fluorescence images of Tetra-Zn<sub>2</sub>BDPA-SR, Bis-Zn<sub>2</sub>BDPA-SR, and Tracer-653 accumulation in a living mouse at 24 h after probe injection (**a**). In vivo fluorescence images at earlier time points are shown in Figure S5. Representative ex vivo fluorescence images of cryoinjured brains containing Tetra-Zn<sub>2</sub>BDPA-SR, Bis-Zn<sub>2</sub>BDPA-SR, or Tracer-653 (**b**).